Supporting information

Highly-dispersed ZrO_x modulates C-O bond activation for boosting CO_2 hydrogenation to higher alcohols

Lingfeng Wang,[a,b] Tangkang Liu,[a,b,*] Mengqi Hu,[a,b] Peng Peng,[a,b] GuoLiang Liu,[a,b,*] Anmin Zheng[a,b,*]

Methods

Synthesis of catalysts

Zr-CuFe catalyst precursors with varying zirconium contents were synthesized *via* the chemical precipitation method. Specifically, 2.42 g of copper nitrate, 4.04 g of iron nitrate, and a designated amount of zirconium nitrate pentahydrate were dissolved in 100 mL of deionized water. In a separate container, 7.95 g of Na_2CO_3 was dissolved in 100 mL of deionized water. The salt solution was then slowly added dropwise into the vigorously stirred alkaline solution. After complete addition, the mixture was continuously stirred at room temperature for 20 minutes. The resulting precipitate was repeatedly washed and settled using 3000 mL of deionized water to ensure thorough removal of sodium ions. The sample was subsequently dried overnight in a vacuum oven at 80°C, followed by grinding to obtain the Zr(x%)-CuFe precursor.

Zr(4%)-K(y%)CuFe catalysts with different potassium loadings were prepared *via* the incipient wetness impregnation method. In a typical procedure, 1 g of the Zr(4%)-CuFe powder was uniformly dispersed in 3 mL of an aqueous K_2CO_3 solution. The mixture was stirred at room temperature for 2 hours to facilitate impregnation, followed by drying *via* rotary evaporation. The resulting solid powder was then calcined in a muffle furnace at 400°C for 4 hours (with a heating rate of 2°C/min) under static air, yielding the final Zr(x%)-K(y%)CuFe catalyst.

Catalyst evaluation

The activity evaluation was carried out on a fixed-bed stainless steel microreactor. Before testing, 200 mg of the catalyst was thoroughly mixed with 400 mg of quartz sand, then the Mixture was reduced in a 10 vol% H_2/Ar stream (30 mL min^{-1}) at 320 °C for 1 hour, and then a reactant (CO_2/H_2=1/3 by volume, 4 vol% N_2 as an internal standard, and GHSV of 3 L g_{cat}^{-1} h^{-1}) was inducted into the reactor to pressurize to 4.0 MPa. Afterwards, the evaluation was performed at 320 ℃. The effluent products (such as N_2, CO_2, CO, methanol, C_{2+} alcohols, alkanes, and alkenes) were analyzed online by a gas chromatograph equipped with a flame ionization detector (FID, CB-Plot Q capillary column) and a thermal conductivity detector (TCD, TDX-01 column).

The CO_2 conversion, CO selectivity, CO-free product selectivity, and the proportion of higher alcohols in total alcohols, as well as the STY of alcohol products, are calculated based on Equations 1-5 below.

$$CO_2\ Conversion = \frac{A_{co_2,in} - A_{co_2,out}}{A_{co_2,in}} \times 100\% \quad (1)$$

$$CO\ Selectivity = \frac{A_{CO,out}}{A_{co_2,in} - A_{co_2,out}} \times 100\% \quad (2)$$

$$CO - free\ C_i\ selectivity = \frac{C_{i,out} \times i}{\sum_{i=1}^{n} C_{i,out} \times i} \times 100\% \quad (3)$$

$$C_{2+}OH/ROH\ Fraction = \frac{\sum_{i=2}^{n} C_iOH_{out} \times M_i}{\sum_{i=1}^{n} C_iOH_{out} \times M_i} \times 100\% \quad (4)$$

$$The\ STY\ of\ C_iOH = \frac{C_{CO_2} \times Cov_{CO_2} \times Sel_{C_iOH} \times M_i \times GHSV}{22.4 \times i} \quad (5)$$

where $A_{co_2,in}$ and $A_{co_2,out}$ represent the chromatographic peak areas of CO_2 at the inlet and outlet, respectively, $A_{CO,out}$ represents the chromatographic peak area of CO at the outlet, $C_{i,out}$ denotes the carbon molar number and carbon number of carbon product (C_i) at the outlet, C_iOH_{out} and M_i represent the molar amount and corresponding molar mass of alcohol products at the outlet, C_{CO_2} represents the initial concentration of CO_2, Cov_{CO_2} denotes the conversion rate of CO_2, Sel_{C_iOH} indicates the selectivity of the corresponding alcohol product, and GHSV represents the space velocity employed in the catalyst evaluation.

Characterizations. TEM images were performed on a Titan G2 F30 S-TWIN. X-ray diffraction pattern was carried out on a Rigaku Miniflex600 powder diffractometer (40 kV and 15 mA) equipped with Cu Kαradiation. The N_2 adsorption-desorption experiments were measured by using a Micromeritics ASAP-2020 Analyzer. X-ray photoelectron spectroscopy was recorded on a Thermo Scientific ESCALAB 250Xi X-ray photoelectron spectrometer (15 kV and 10 mA) equipped with a monochromatic Al K*α* source (*hv*=1486.6 eV). The metal content was detected by ICP-AES (inductively coupled plasma-atomic emission spectrometry) on an IRIS Intrepid II XSP (Thermo Elemental) instrument.

H_2-TPR measurements. It was measured using a Micromeritics Autochem 2920 instrument. Typically, 30 mg of catalyst was loaded into a U-type quartz tube and pretreated in a high-purity Ar flow (30 mL min^{-1}) at 150 °C for 1 h. After cooling to room temperature, the atmosphere was switched to 5 vol% H_2/Ar (30 mL min^{-1}) and purged for 10 min. The temperature was then increased to 800 °C at a heating rate of 10 K min^{-1}, and the signal was recorded by a thermal conductivity detector (TCD).

CO pre-adsorbed H_2 temperature-programmed surface reaction mass spectrometry (H_2-TPSR-MS). It was conducted on a Micromeritics Autochem 2920 instrument coupled with an online Hiden QIC-20 mass spectrometer. The catalyst (30 mg) was placed in a U-type quartz tube and pre-reduced in 5 vol% H_2/Ar (30 mL min^{-1}) at 320 °C for 1 h, followed by cooling to

ambient temperature. The gas was then switched to 5 vol% CO/Ar (30 mL min^{-1}) for 1 h, after which the tube was flushed with high-purity Ar (30 mL min^{-1}) for 30 min. Finally, the MS signals for H_2, CO, CO_2, and CH_4 were recorded while heating from 30 to 800 °C at 10 K min^{-1}.

CO or CH_3CHO pulse transient hydrogenation measurements. The spent catalyst was first reactivated in a CO_2/H_2 stream (H_2/CO_2 = 3, 20 mL min^{-1}) at 320 °C for 2 h, then purged with pure Ar for 1 h. A 5 vol% H_2/Ar stream (30 mL min^{-1}) was used as the carrier gas, and pulses of CO or CH_3CHO were introduced into the reactor for several cycles at 10 min intervals. The MS signals for CO, CH_4, CH_3CHO, and CH_3CH_2OH (or for CH_3CHO and CH_3CH_2OH in the case of acetaldehyde pulsing) were collected.

CO_2-temperature-programmed desorption (CO_2-TPD). Approximately 30 mg of the catalyst was placed in a quartz tube and first reduced under a 5 vol% H_2/Ar flow at 320 °C for 1 hour with a heating rate of 3 K min^{-1}. After reduction, the atmosphere was switched to Ar to cool the sample to ambient temperature. Subsequently, pure CO_2 was introduced and allowed to adsorb for 30 minutes, followed by purging with Ar for 30 minutes. Finally, the temperature was raised to 800 °C at a rate of 10 K min^{-1}, and the desorbed species were monitored using a mass spectrometer (tracking the MS signal of CO_2).

***In situ* DRIFTS spectra of the CO_2+H_2 reaction.** The catalyst (10 mg) was loaded into an *in situ* IR cell and pre-reduced at a heating rate of 3 K min^{-1} for 1 h. After cooling to the target temperature (200 and 250 °C) and collecting the background spectra, a CO_2/H_2 mixture (1:3 by volume) was introduced at 30 mL min^{-1} and 0.3 MPa. Time-resolved DRIFTS spectra were recorded concurrently under these conditions.

***In situ* Raman spectra of the CO_2+H_2 reaction.** 20 mg of catalyst was loaded into the *in situ* cell of a Renishaw inVia Qontor instrument. The system was first purged with a 10 vol% H_2/Ar, followed by temperature ramping to 320 °C at a heating rate of 3 K min^{-1}, and maintained at this temperature for 1 hour to reduce the catalyst. After reduction, the gas was switched to a $CO_2/H_2/N_2$ mixture (molar ratio of 6:18:1) at a reaction pressure of 0.1 MPa. Raman spectra were collected synchronously using a 325 nm laser operating at 10 mW with an exposure time of 10 seconds per spectrum.

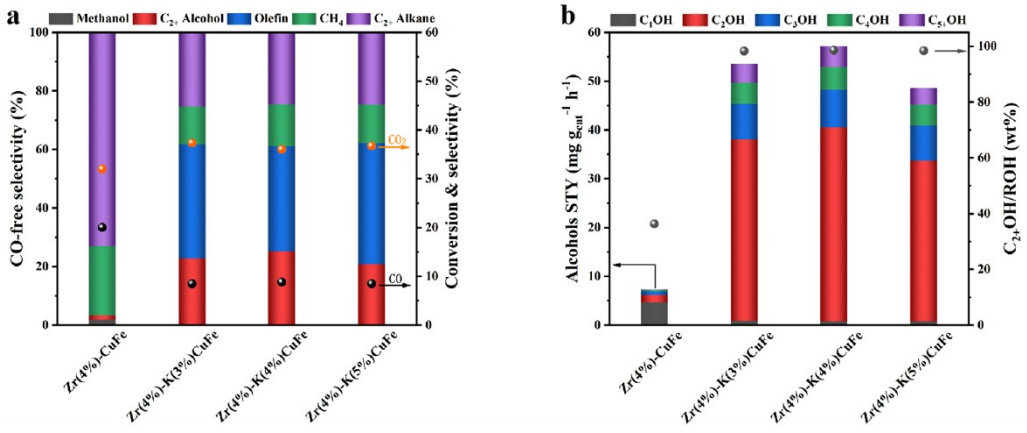

Figure S1. Catalytic performance of the Zr(4%)-K(y%)CuFe catalysts. (a) CO_2 conversion and carbon product selectivity (including methanol, higher alcohols, olefins, methane, C_{2+} alkanes, and CO). (b) Space-time yield (STY) of total alcohols and the mass fraction of higher alcohols among the total alcohol products. Reaction conditions: 320 ℃, 4 MPa, and 3 L g_{cat}^{-1} h^{-1}.

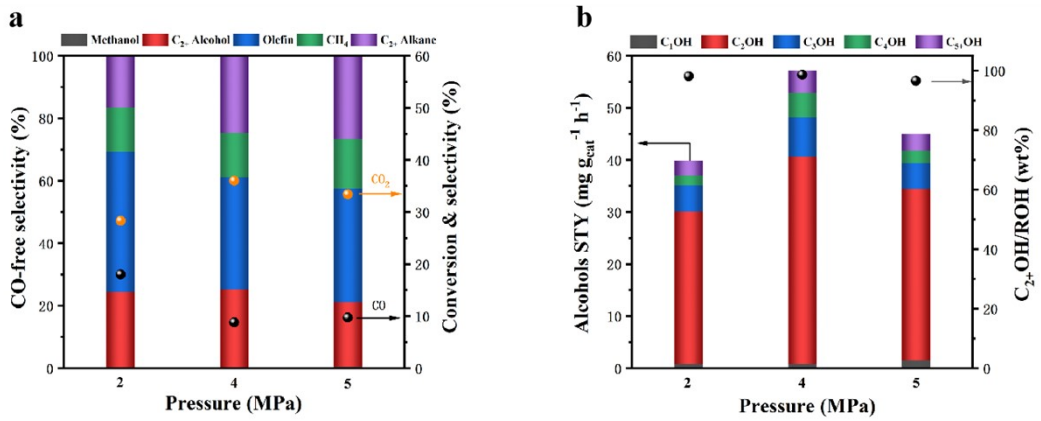

Figure S2. (a) CO_2 conversion and carbon product selectivity (including methanol, higher alcohols, olefins, methane, C_{2+} alkanes, and CO) at different reaction pressures. (b) Space-time yield (STY) of alcohols and the mass fraction of higher alcohols in the total alcohol products at different pressures.

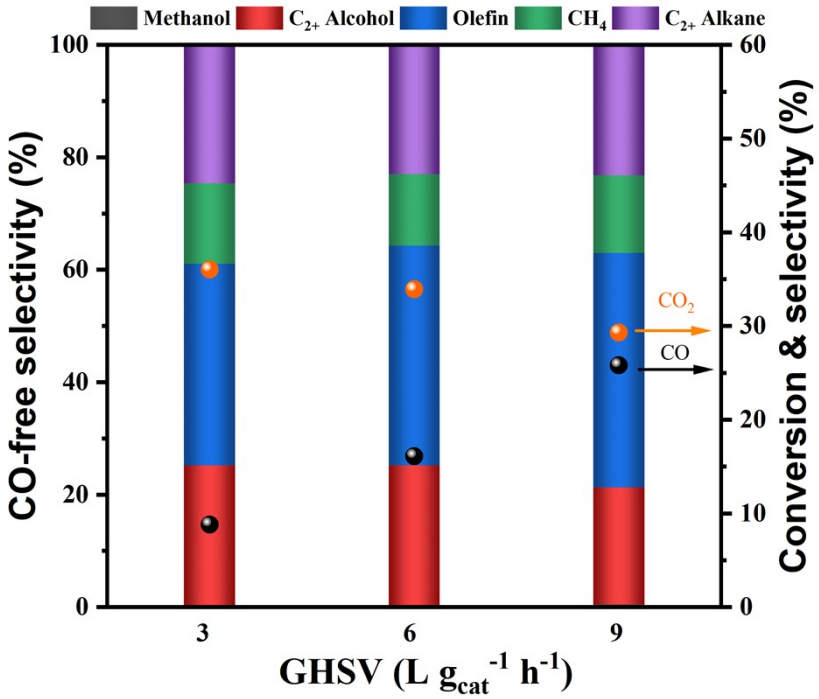

Figure S3. CO_2 conversion and carbon product selectivity (including methanol, higher alcohols, olefins, methane, C_{2+} alkanes, and CO) at different gas hourly space velocities.

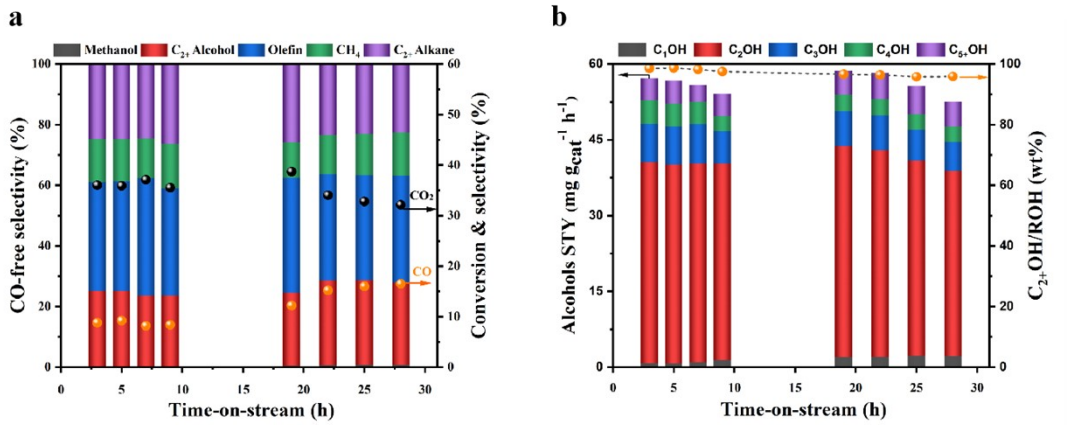

Figure S4. Catalytic stability test of the Zr(4%)-KCuFe catalyst under conditions of 320 ℃, 4 MPa, and 3 L g_{cat}^{-1} h^{-1}.

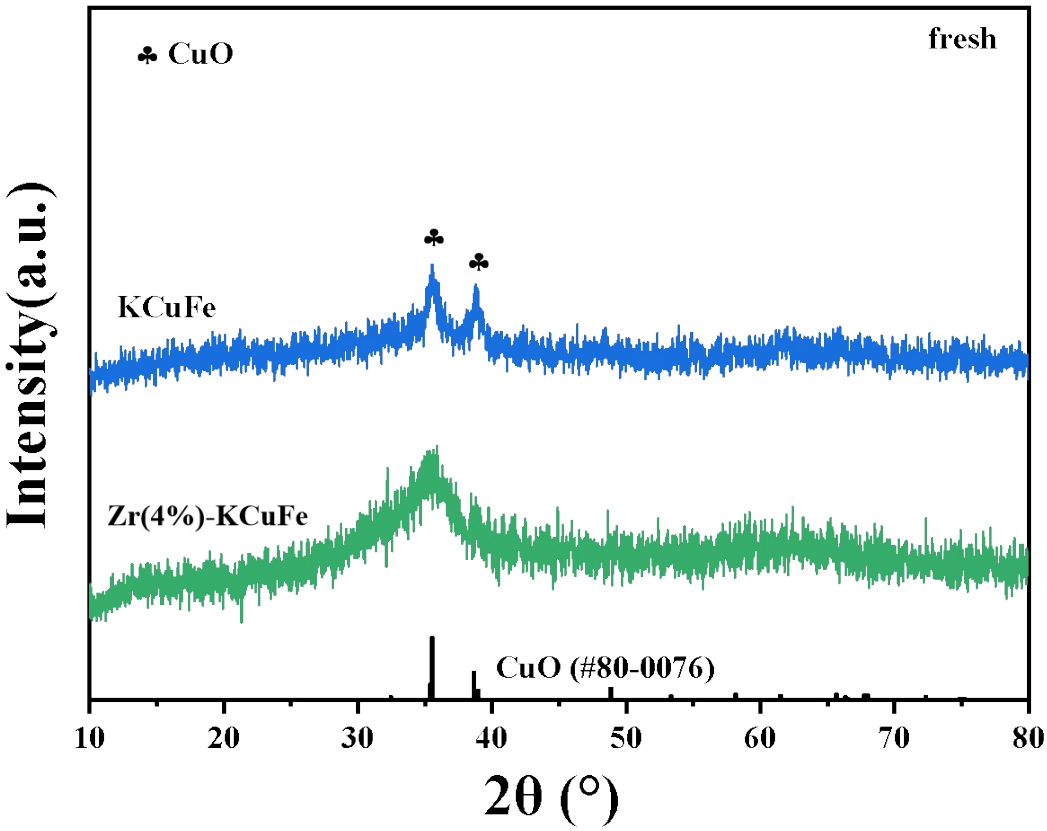

Figure S5. XRD patterns of the fresh KCuFe and Zr(4%)-KCuFe catalysts.

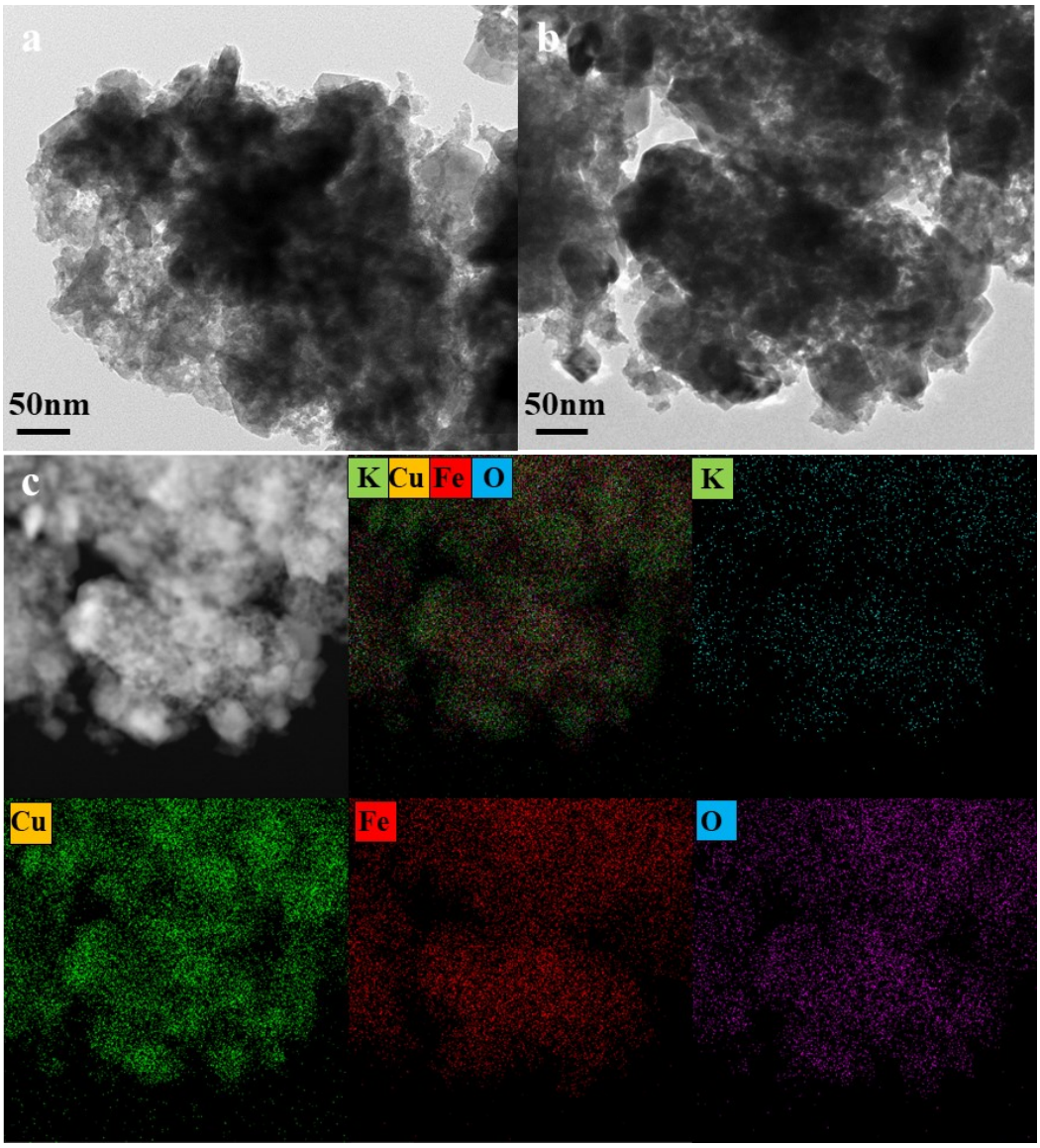

Figure S6. (a,b) TEM images, (c) HAADF-STEM image and the corresponding energy-dispersive X-ray (EDX) spectroscopy elemental maps of the KCuFe catalyst.

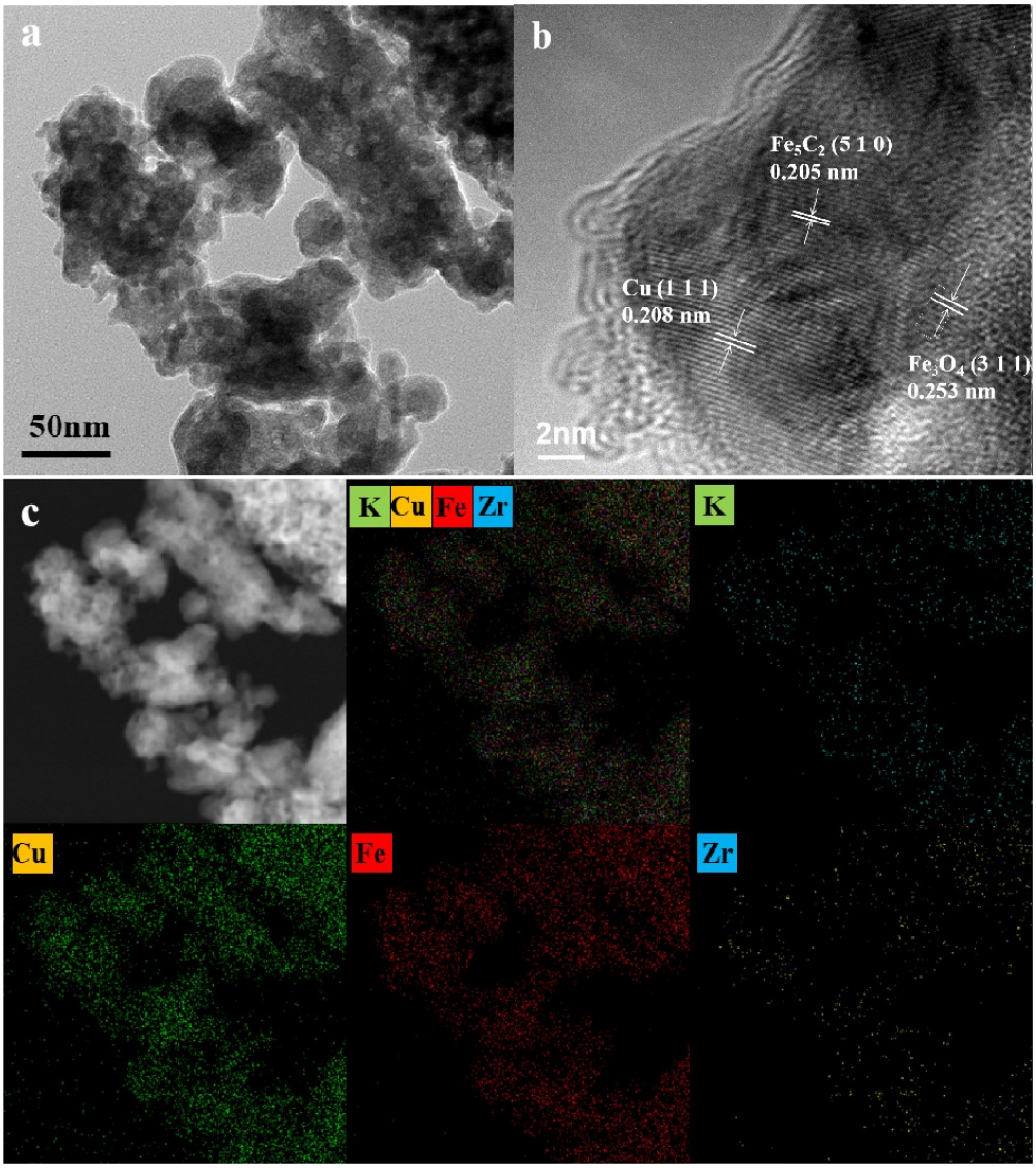

Figure S7. (a) TEM image, (b) HRTEM image, and (c) the corresponding energy-dispersive X-ray (EDX) spectroscopy elemental mapping of the Zr(4%)-KCuFe catalyst.

Table S1. Comparison of the catalytic activity from CO_2 hydrogenation to higher alcohols (HA) in the fixed-bed reactor over our catalyst with advanced catalysts reported in the literature.

Catalyst	T (°C)	P (MPa)	GHSV (mL g_{cat}^{-1} h^{-1})	H_2/CO_2	X_{CO2} (%)	S_{CO} (%)	S_{HC} (%)	S_{MeOH} (%)	S_{HA} (%)	HA yield (%)	Ref.
$Co/La_4Ga_2O_9$	270	3.5	3 000	3	4.6	15.4	40.9	23.4	41.0	1.6	1
$2.5K5Co\text{-}In_2O_3$	380	4	2 250	3	36.6	80.8	33.9	1.7	11.3	4.1	2
$CoMoC_x$-800	180	2	-	3	-	0.5	0.0	0.5	99.5	-	3
CoCu/MCM-41	200	4	-	3	-	0	0	14.7	85.3	-	4
0.19Na-Rh@S-1	250	5	6 000	3	10	32	36.0	34.2	23.9	1.7	5
$Ir_1\text{-}In_2O_3$	240	6	-	5	-	0	0	<1	99.7	-	6
K-0.82-FeIn/Ce-ZrO_2-900	300	10	4 500	3	29.6	13.4	61.4	10.0	30.1	8.5	7
KFeRh-SiO_2	250	7.5	7 000	3	18.4	~18	~72.1	~17.1	17.1	2.9	8
Na/Fe_3O_4	300	3	2 500	3	30.6	4.1	56.3	2.8	41.1	12.4	9
FeNaS-0.6	320	3	8 000	3	32	20.7	83.9	0.6	12.6	4	10
0.6S-KCFZ	320	5	3 000	3	32	~12	~76.5	~1.5	20.3	~6.4	11
Cr(1%)-CuFe	320	4	6 000	3	38.4	14.8	~70.0	~1.7	25.1	9.6	12
KFeCu/*a*-ZrO_2	320	4	3 000	3	32.3	15.1	70.2	1.7	24.8	8.0	13
CZA(1)/K-CMZF(1)	320	5	6 000	3	42.3	13.8	78.3	4.0	17.6	7.4	14
Na-Fe@C/K-CuZnAl	320	5	4 500	2.8	39.2	9.4	54.5	8.3	38.6	14.5	15
Co_2C||CuZnAl	250	5	12 000	3	21.2	~31	~72.5	~1.4	18.4	3.9	16
FeCuGaZn-0.75	340	5	6000	3	26	~15	~60.6	~1.0	23.2	6	17
Zr(4%)-KCuFe	320	4	3000	3	36	8.8	74.7	0.2	25.1	8.2	This work
			6000		33.9	16.1	74.8	0.4	24.8	7.1	

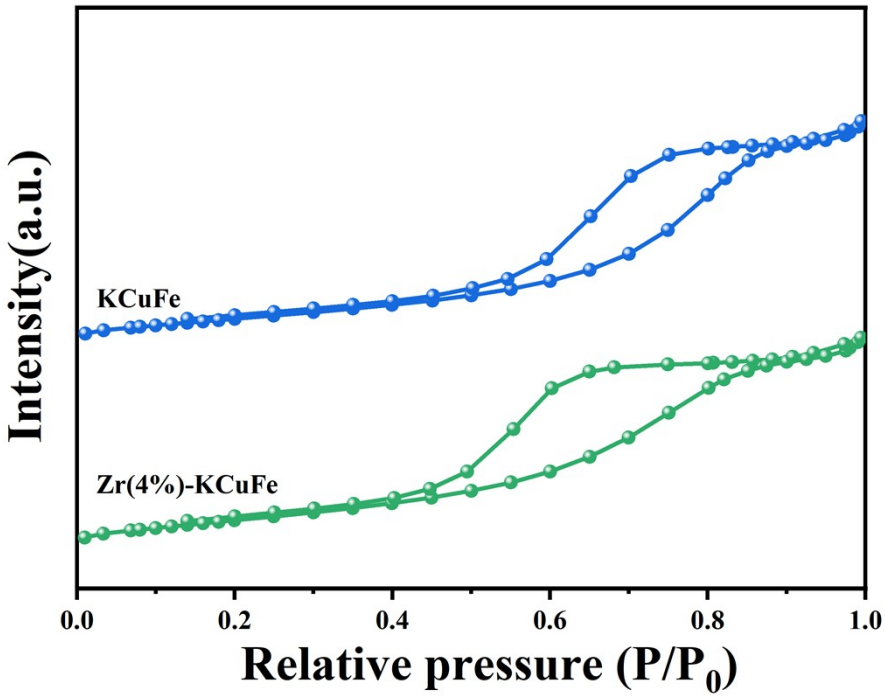

Figure S8. N_2 adsorption-desorption isotherms of the KCuFe and Zr(4%)-KCuFe catalysts.

Table S2. Structural properties of the KCuFe and Zr(4%)-KCuFe catalysts.

Catalysts	S_{BET} ($m^2 g^{-1}$)	V_{pore} ($cm^3 g^{-1}$)	D_{pore} (n)	K content (wt%)	Zr content (wt%)
KCuFe	51	0.12	6.0	4.5	-
Zr(4%)-KCuFe	60	0.12	4.6	4.4	4.2

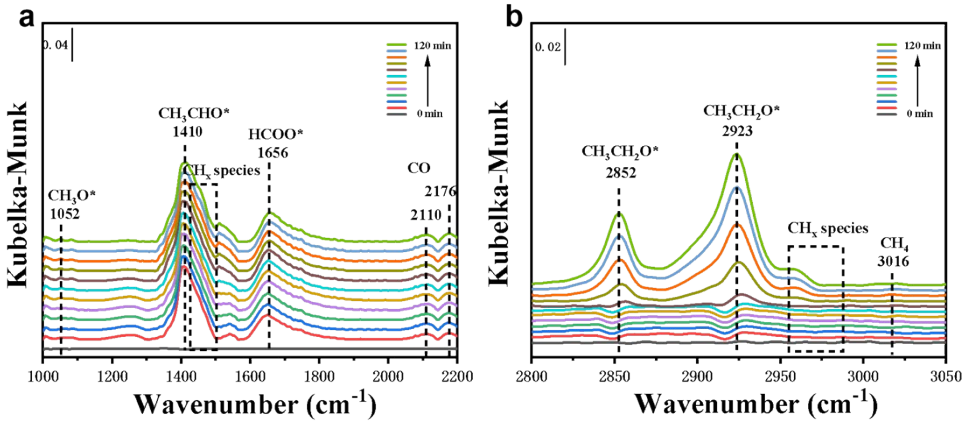

Figure S9. (a,b) *In situ* DRIFTS spectra of the Zr(4%)-KCuFe catalyst. Reaction conditions: 0.3 MPa, 250 °C, H_2/CO_2=3, ca. 30 mL min^{-1}.

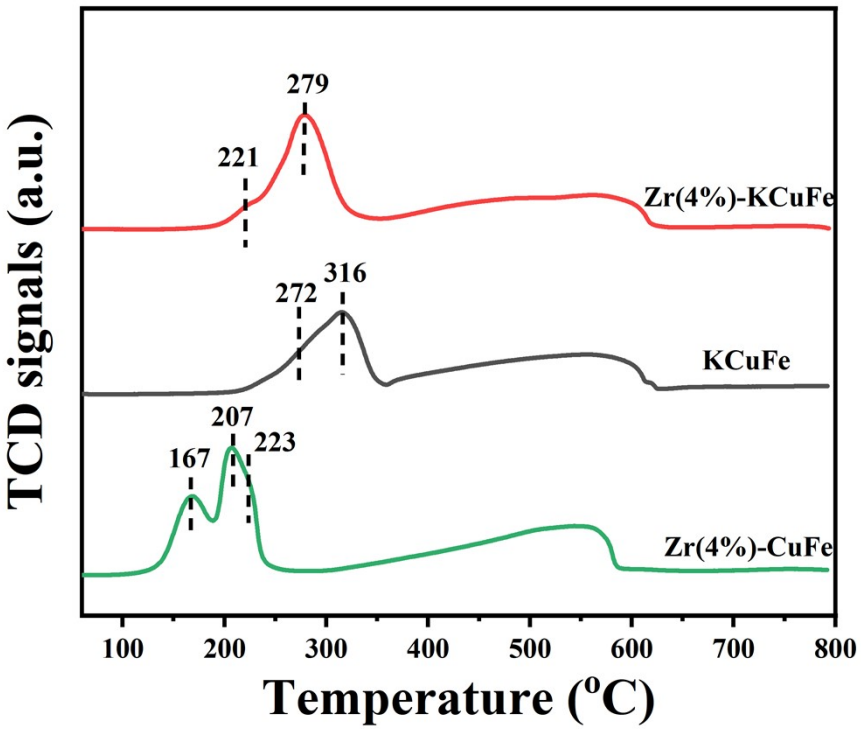

Figure S10. H_2-TPR profiles of the fresh Zr(4%)-CuFe, KCuFe, and Zr(4%)-KCuFe catalysts.

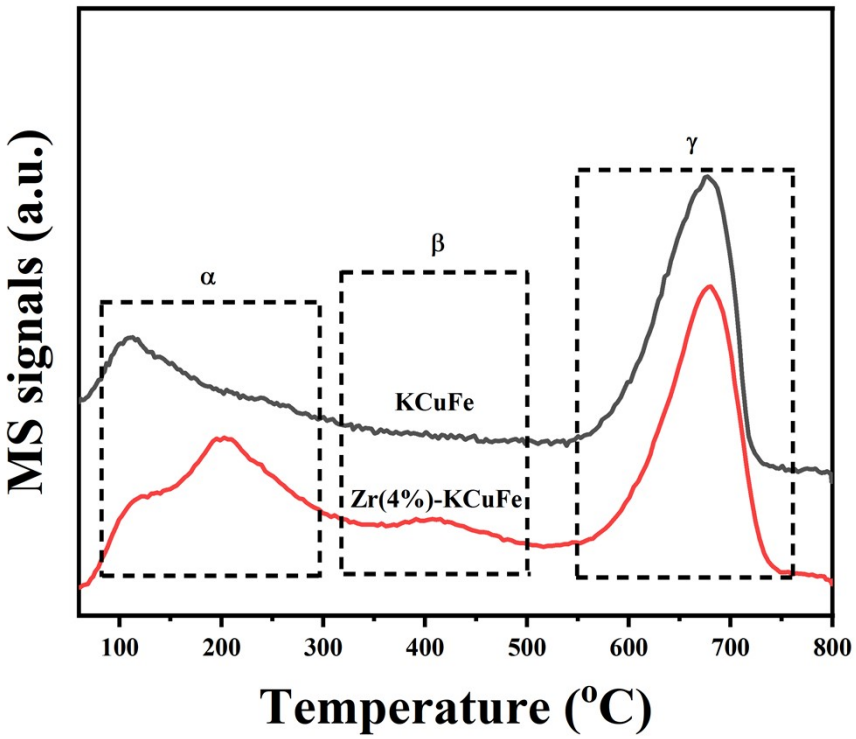

Figure S11. CO_2-TPD profiles of the KCuFe and Zr(4%)-KCuFe catalysts.

Table S3. The corresponding CO_2 desorption peak areas in CO_2-TPD profiles.

Catalysts	A_{CO2} (*10E-7 a.u.)
KCuFe	3.5
Zr(4%)-KCuFe	6.9

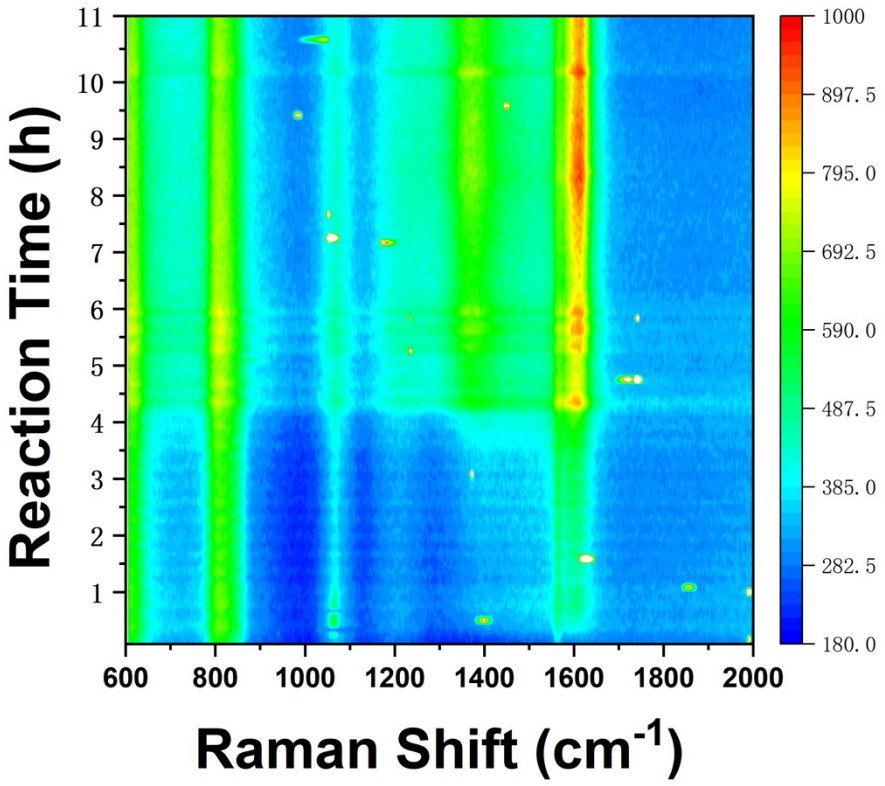

Figure S12. *In-situ* Raman heatmap of the Zr(4%)-KCuFe from 0~11 hours. Reaction conditions: 0.3 MPa, H_2/CO_2=3, and 320 °C.

Table S4. CO_2 and CH_4 desorption peak areas, their corresponding area ratio from CO-TPSR measurements, and the C_{2+} alcohol to C_{2+} hydrocarbon selectivity ratio of the catalysts.

Catalysts	A_{CO2} (*10E-8 a.u.)	A_{CH4} (*10E-8 a.u.)	A_{CO2}/A_{CH4}	C_{2+} alcohols/C_{2+} hydrocarbons
KCuFe	3.52	3.49	1.01	0.31
Zr(4%)-KCuFe	7.91	4.84	1.63	0.42

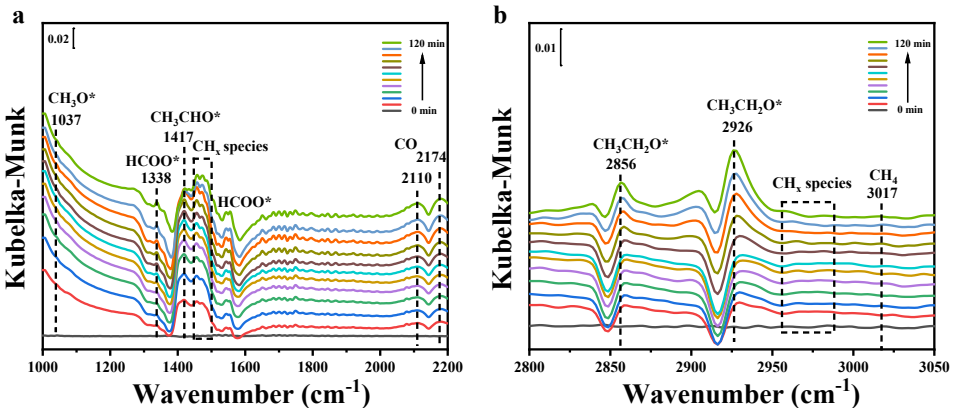

Figure S13. (a,b) *In situ* DRIFTS spectra of the KCuFe. Reaction conditions: 0.3 MPa, 250 °C, H_2/CO_2=3, ca. 30 mL min^{-1}.

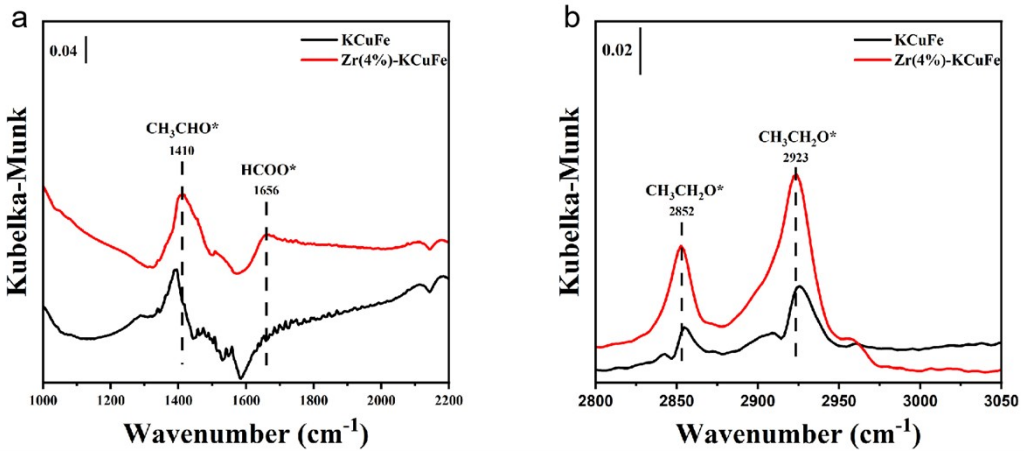

Figure S14. (a,b) *In situ* DRIFTS spectra of KCuFe and Zr(4%)-KCuFe recorded at 250 °C after 120 minutes of reaction. Reaction conditions: 0.3 MPa, H_2/CO_2=3, ca. 30 mL min^{-1}.

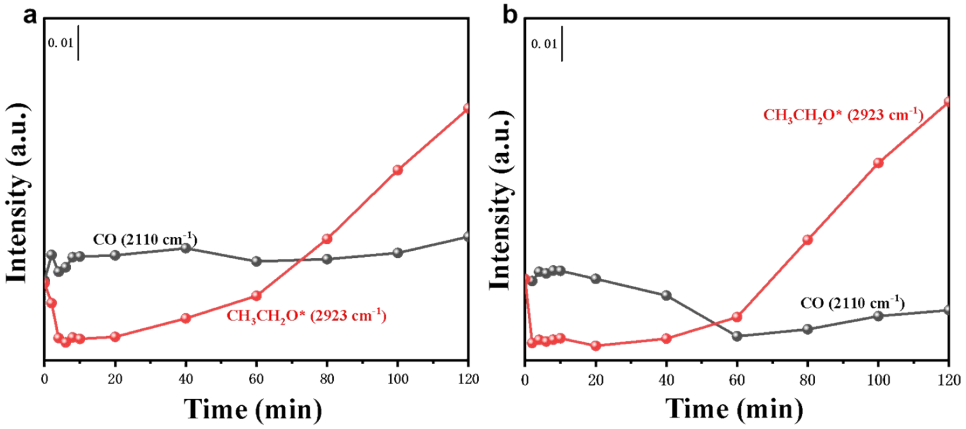

Figure S15. Evolution of IR spectral intensity as a function of reaction time over the (a) KCuFe and (b) Zr(4%)-KCuFe catalysts. Reaction conditions: 0.3 MPa, 250 °C, $H_2/CO_2 = 3$, ca. 30 mL min^{-1}.

References

1. K. An, S. Zhang, J. Wang, Q. Liu, Z. Zhang, and Y. Liu, *J. Energy. Chem.,* 2021, **56**, 486-495.
2. T. Witoon, T. Numpilai, S. Nijpanich, N. Chanlek, P. Kidkhunthod, C. K. Cheng, K. H. Ng, D.-V. N. Vo, S. Ittisanronnachai, C. Wattanakit, M. Chareonpanich, and J. Limtrakul, *Chem. Eng. J.,* 2022, **431**, 133211.
3. H. Zhang, H. Han, L. Xiao, and W. Wu, *ChemCatChem,* 2021, **13**, 3333-3339.
4. Z. Wang, C. Yang, X. Li, X. Song, C. Pei, Z.-J. Zhao, and J. Gong, *Nano Res.,* 2023, **16**, 6128-6133.
5. F. Zhang, W. Zhou, X. Xiong, Y. Wang, K. Cheng, J. Kang, Q. Zhang, and Y. Wang, *J. Phys. Chem. C.,* 2021, **125**, 24429-24439.
6. X. Ye, C. Yang, X. Pan, J. Ma, Y. Zhang, Y. Ren, X. Liu, L. Li, and Y. Huang, *J. Am. Chem. Soc.,* 2020, **142**, 19001-19005.
7. X. Xi, F. Zeng, H. Zhang, X. Wu, J. Ren, T. Bisswanger, C. Stampfer, J. P. Hofmann, R. Palkovits, and H. J. Heeres, *ACS Sustainable Chem. Eng.,* 2021, **9**, 6235-6249.
8. A. Goryachev, A. Pustovarenko, G. Shterk, N. S. Alhajri, A. Jamal, M. Albuali, L. van Koppen, I. S. Khan, A. Russkikh, A. Ramirez, T. Shoinkhorova, E. J. M. Hensen, and J. Gascon, *ChemCatChem,* 2021, **13**, 3324-3332.
9. F. Lu, X. Chen, W. Wang, and Y. Zhang, *Catal. Sci. Technol.,* 2021, **11**, 7694-7703.
10. R. Yao, J. Wei, Q. Ge, J. Xu, Y. Han, Q. Ma, H. Xu, and J. Sun, *Appl. Catal., B,* 2021, **298**, 120556.
11. Y. Wang, X. Zhang, X. Hong, and G. Liu, *ACS Sustainable Chem. Eng.,* 2022, **10**, 8980-8987.
12. Q. Zhang, S. Wang, R. Geng, P. Wang, M. Dong, J. Wang, and W. Fan, *Appl. Catal., B,* 2023, **337**, 123013.
13. T. Liu, D. Xu, M. Song, X. Hong, and G. Liu, *ACS Catal.,* 2023, **13**, 4667-4674.
14. D. Xu, H. Yang, X. Hong, G. Liu, and S. C. Edman Tsang, *ACS Catal.,* 2021, **11**, 8978-8984.
15. Y. Wang, K. Wang, B. Zhang, X. Peng, X. Gao, G. Yang, H. Hu, M. Wu, and N. Tsubaki, *ACS Catal.,* 2021, **11**, 11742-11753.
16. S. Zhang, C. Huang, Z. Shao, H. Zhou, J. Chen, L. Li, J. Lu, X. Liu, H. Luo, L. Xia, H. Wang, and Y. Sun, *ACS Catal.,* 2023, **13**, 3055-3065.
17. Y. Ma, Y. Liu, Z. Huang, X. Han, L. Ye, X. Qin, H. Xu, L. Kong, J. Li, J. Zhang, X. Pu, and J. Liu, *Sep. Purif. Technol.,* 2025, **364**, 132583.